MRS Communications (2018), 1 of 6

doi:10.1557/mrc.2018.149

MRS Communications

Research Letter

Direct visualization of nano and microscale polymer morphologies in as-prepared and dialyzed polyampholyte hydrogels by electron microscopy techniques

Xinda Li, Hemant Charaya, and **Thuy Nguyen Thanh Tran,** Department of Chemical and Materials Engineering, University of Alberta, Edmonton, Alberta T6 G 1H9, Canada
Byeongdu Lee, Advanced Photon Source, Argonne National Laboratory, Argonne, Illinois 60439, USA
Jae-Young Cho, National Research Council of Canada (NRC), 11421 Saskatchewan Drive NW, Edmonton, Alberta T6 G 2M9, Canada
Hyun-Joong Chung, Department of Chemical and Materials Engineering, University of Alberta, Edmonton, Alberta T6 G 1H9, Canada
Address all correspondence to Hyun-Joong Chung at **chung.hj13@ualbrerta.ca**

(Received 25 May 2018; accepted 24 July 2018)

Abstract

The structure of polymer networks in hydrogels determines the properties. In this study, we investigated the structure of a charge-balanced polyampholyte, poly(4-vinylbenzenesulfonate-*co*-[3-(methacryloylamino) propyl] trimethylammonium chloride). From as-prepared samples, nanoscale globules were visualized in polyampholyte hydrogels for the first time. The impact of dialyses processes on polymer structures were also studied. In deionized water, salt ions are leached out, thus polymer chains undergo *zipping* process to form cellular structure with micrometer-thick polymer walls that allow mechanical toughness to the hydrogel. Samples dialyzed in 6 M potassium hydroxide solution did not show such cellular structure, as in the case of as-prepared samples.

Introduction

Electron microscopy (EM) has been actively used in elucidating structures of polymeric materials. Microscopic techniques are especially useful when the polymer has periodic nanostructures (e.g., block copolymers),[1] when the polymer contains inorganic substances[2] or ionic clusters[3] to prevent detrimental electronic charge accumulation, and when the polymer is semicrystalline.[4] Recently, advanced transmission electron microscope (TEM) enabled single-chain imaging of polymers under specific conditions.[5] For hydrogels, nanoscale molecular and supramolecular structures have mostly been probed by indirect methods, such as small-angle neutron scattering, small-angle x-ray scattering (SAXS), and light scattering.[6,7] To visualize the micrometer-scale fibrous network structures of hydrogels, a protocol of cryogenic quenching, followed by freeze-drying for scanning electron microscope (SEM) imaging was established.[8] An advanced EM technique of cryo-TEM and -SEM has also been used for gel samples,[9] but direct EM imaging of hydrogel nanostructure has been available in specific cases, such as thin film gels[10] or ultramicrotomed gels that contain inorganic particles.[11]

Polyampholytes, a subclass of polyelectrolytes, are macromolecules carrying ionizable functional groups that dissociate and leave positively and negatively charged groups on the polymer chain under certain conditions, for example, in the presence of water.[12,13] The hydrogel of polyampholyte is formed by the ionic cross-linking between the chains due to local non-zero net charge in concentrated polyampholyte solution.[12] The reversible behavior of ionic interactions in the polyampholyte dedicates to the self-healing ability of the hydrogel. For example, the hydrogel sample broken into two pieces can be stored in a concentrated salt solution and bind together after leaching out the salt.[14] Moreover, the upper critical solution temperature of polyampholyte hydrogel can be manipulated by tuning the strength of ionic interactions.[15] Based on these unique properties of ionic cross-linking, polyampholyte hydrogels have been used as electrolyte for flexible and self-healing supercapacitors,[16] and as an optically modulating substance for thermosensitive smart windows.[17] Such diverse applications of polyampholyte hydrogels are possible by controlling morphology. The morphology of polyampholyte hydrogels, however, has seldom been studied. Thus, it is important to study its morphology at nanoscopic and microscopic scales using advanced microscopy techniques.

Fundamentally speaking, visualizing the smallest morphologic building block is an important issue. Polyampholyte solutions are theoretically predicted to form a globular network structure.[12,13,18] Based on the light-scattering and -swelling experiments, Nisato et al. suggested the existence of the globular structure in polyampholyte hydrogels.[19] Recently, we found a strong evidence that such globular network structure exists in hydrogels; our SAXS results indicated a networked globule structure in the charge-balanced polyampholyte hydrogels, where the unit globules have an average radius of gyration

of ~2.5 nm.[20] Such globular structure is consistent with theoretical prediction based on Debye–Huckel fluctuation-induced attraction model.[12,13] However, the existence of the globules have not been supported by direct microscopic visualization techniques to the best of our knowledge.

Visualizing the impact of dialyzing solutions on the microscopic polymer structure in polyampholyte hydrogels is another important issue. In most applications, hydrogels are submerged in a solution environment that is different from its as-prepared condition. The solution environment modulates physical and chemical properties. For example, as-prepared polyampholyte hydrogels are dialyzed in deionized water (DIW) to achieve high toughness by forming ion complexes between the oppositely charged groups in polyampholyte backbones.[21,22] Another example is dialysis in aqueous solution of potassium hydroxide (KOH) to introduce mobile ions in the hydrogel as the charge carriers for the ionic conduction to achieve gel electrolyte for electrochemical energy storage devices.[16] While it is well known that polymer structures govern the physical and chemical properties of hydrogels, the morphologic impact on the dialysis processes in different solutions have not been studied to date.

In this study, we show microscopic evidence of the nanoscale globules in the as-prepared polyampholyte hydrogels for the first time using a low-dose field-emission SEM (FE-SEM) and scanning transmission electron microscopy (STEM). Here, the thermal expansion difference between the polymer sample (freeze-dried) and metallic coating (for charge dissipation), as well as high salt concentration present in the freeze-dried polymer sample, makes such FE-SEM imaging possible for polyampholyte hydrogels. Another major finding in this paper is the microscopic morphologic impact on dialyses processes, which are necessary to convert the as-prepared polyampholyte hydrogels into practical advanced materials. Specifically, we studied the effect of DIW and the 6 M solution of KOH dialyses, respectively. Here, microscopic cellular structures were observed in the DIW-dialyzed sample, whereas there is no visible macroscopic structure in the KOH-dialyzed sample. This morphologic observation is consistent with high mechanical strength[21,22] and high low-temperature ionic conductivity,[16,20] respectively, reported in previous literatures.

Experimental methods

Polyampholyte hydrogel synthesis and dialysis

The protocol of polyampholyte synthesis was described in previous works.[20,22] Briefly, 1 M sodium 4-vinylbenzenesulfonate (NaSS) and 1 M [3-(methacryloylamino)propyl] trimethylammonium chloride (MPTC) with Irgacure 2959 (photoinitiator, 0.25 mol%, compared with the total concentration of NaSS and MPTC) and NaCl were dissolved in DIW to form the precursor solution (see Table I for the sample details). In the precursor solution, NaCl concentration is 10 wt.%. Dialysis processes were carried out on as-prepared PA-10-2.1 samples. PA-10-2.1 samples were dialyzed in abundant DIW for 1 week to prepare D-PA-10-2.1. PA-10-2.1 samples were dialyzed in 6 M KOH aqueous solution for 1 week to prepare K-PA-10-2.1.

Freeze-drying of polyampholyte hydrogel

Polyampholyte hydrogel samples were freeze-dried before SEM characterization. For PA-10-2.1, the samples were cooled from room temperature to −20 °C at a rate of 0.5 °C/min using a temperature-controlled chamber, and held at the desired temperature for 30 min. After that, the samples were taken from the chamber, and then immediately quenched in liquid nitrogen, followed by a complete dehydration in a freeze-dryer (Super Modulyo, Savant, MA, USA). For D-PA-10-2.1 and K-PA-10-2.1, the samples were quenched from +20 °C in liquid nitrogen, followed by freeze-drying processes.

SEM imaging

In order to mitigate charging-associated problems in SEM imaging, the freeze-dried hydrogel samples were coated with a 5 nm-thick Au–Pd layer by sputtering. Alloying 20 wt.% of Pd in the sputtering target is a popular choice nowadays because the Pd acts as a physical barrier to prevent Au atoms conglomerating into large islands. SEM images were obtained at 5 kV accelerating voltage, 20 μA emission current, and a working distance of 5 mm on a high-resolution Hitachi S-4800 cold FE-SEM. For low-dose methods, image acquiring time was <20 s. For SEM images in the "Hydrogel structures of sample dialyzed in DIW and KOH" section, a FE-SEM (Sigma, Zeiss) was utilized for the morphologic study.

STEM imaging

STEM samples were prepared by depositing the freeze-dried and ground hydrogel sample powders on a carbon-coated 400-mesh copper grid (Electron Microscopy Sciences). STEM imaging were performed at 30 kV acceleration voltage and 30 μA emission current on Hitachi S-5500 ultra-high-resolution SEM.

Table I. List of the samples prepared.

Sample[a]	NaSS conc (M).	MPTC conc. (M)	NaCl conc. (wt.%)	UV time (h)	Further treatment
PA-10-2.1	1.07	1.03	10	8	–
D-PA-10-2.1	1.07	1.03	10	8	Dialyzed in DIW
K-PA-10-2.1	1.07	1.03	10	8	Dialyzed in 6 M KOH

[a]In all cases, 0.25 mol% photoinitiator (compared with the combined concentration of NaSS and MPTC) was added in the precursor solution.

https://doi.org/10.1557/mrc.2018.149

Results and discussion

Globular structures in as-prepared hydrogels

Because inelastic scattering involves "collision" between the incoming electrons and atomic electrons of similar mass, appreciable energy will be transferred to the specimen in the form of heat, giving rise to a local temperature.[23] The interactions of electrons with organic matter also cause radiolysis of organic materials. Radiolysis yields ionization and breaks chemical bonds, and the bond breakage results in a mass loss by escaping of light atoms (particularly hydrogen, nitrogen, and oxygen).[23,24] Thus, the polymer sample is more sensitive to the electron radiation compared with the metallic coating. To alleviate these effects, "low-dose" technique was used to take the images, which means focusing on one place on the sample and taking micrographs of a previously non-irradiated place. The beam is directed to the feature only when it is being recorded.[25] Dose means the total exposure to electrons, which is the product of incident-current density and exposure time.

During our SEM imaging, the gun voltage of 5 kV was used to minimize the radiolysis of the sample. This low acceleration voltage slows down the radiolysis of the polymer sample. After focusing at the adjacent area, the beam was directed to the area of interest, and all FE-SEM images in our study were taken within <20 s. Here, the FE-SEM imaging, which typically causes electron charging and subsequent evaporation of non-conducting polymer chains, was possible as a result of following factors. Firstly, the globular structure was visualized from the "cracks" in the conductive surface "shell" of sputtered Au–Pd coating layer, analogous to pomegranate arils visualized in the cracks of the mature fruit's skin. Here, the 5 nm-thick metallic coating has smaller thermal expansion coefficients compared with polymer materials. Upon the electron incidence, cracks formed occasionally in the Au–Pd coating layer due to local heating, revealing the polymer samples in the crack areas, as schematized in Fig. 1. The exposed polymers enjoyed temporal relief from detrimental charge buildup because adjacent metallic coatings dissipated the incident electrons. Secondly, a large amount of salt in the freeze-dried polyampholyte further reduced the polymer sample's vulnerability against electron beam radiation. Since the sensitivity of the sample to the electron irradiation is related to the content of the organic material component, increasing the amount of inorganic components in the sample can improve the stability of the sample under the electron radiation.[25] In our hydrogels, a large amount of NaCl (approximately 20 wt.% when calculated against polymer contents as $C_{\mathrm{NaCl}} = m_{\mathrm{NaCl}}/(m_{\mathrm{NaCl}} + m_{\mathrm{polymer}}) \times 100\%$, where C_{NaCl} is the concentration of NaCl, m_{NaCl} is the total mass of NaCl, and m_{water} is the mass of water added in the precursor solution) in the freeze-dried PA-10-2.1 sample reduced the vulnerability of the sample to the electron beam radiation. These particular conditions enabled temporal visualization of nanoscale globules by FE-SEM in our study.

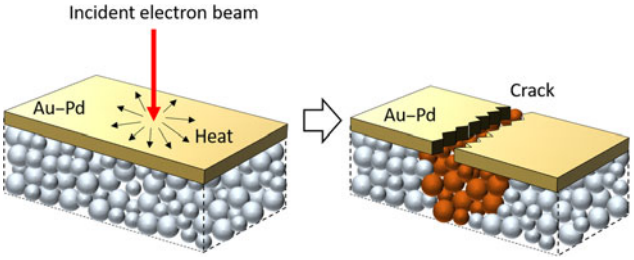

Figure 1. Schematic illustration of crack generation on the polymer and coated metallic layer under electron irradiation.

Figure 2 shows the FE-SEM images of the freeze-dried as-prepared hydrogel (PA-10-2.1). Figure 2 shows the spherical structures in the cracks of Au–Pd coating layer. Although it should be noted that FE-SEM is not a reliable method to determine nanoscopic size of polymeric objects, the diameter of the spherical particles (globules, to our model interpretation) is in a reasonable agreement with the expected average diameter of ~5.2 nm according to SAXS fitting.[20] (It is notable that the radius of a sphere is $\sqrt{5/3}$ times larger than the radius of gyration.) The spherical shape of the globules are attributed to the ionic coacervation of charged polymer chains.[26,27,28] The globule structure is ubiquitous and is indeed the universal primary structure in the charge-balanced polyampholyte hydrogel.

To verify the FE-SEM result, we performed STEM imaging for the ground sample of PA-10-2.1 sample (i.e., powder form).

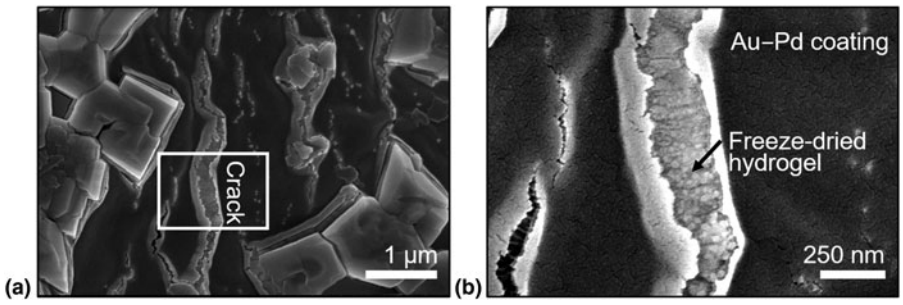

Figure 2. (a) The SEM image of freeze-dried polyampholyte hydrogel (PA-10-2.1). (b) Magnified images of the small region identified in (a).

https://doi.org/10.1557/mrc.2018.149

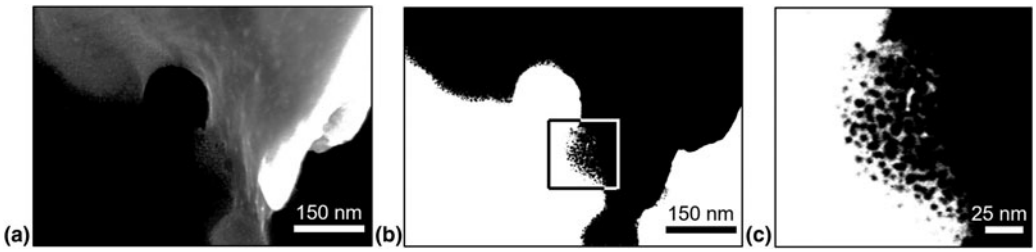

Figure 3. (a) The STEM image of the edge of a freeze-dried polyampholyte hydrogel powder. (b) An alternative view of the image in (a) by introducing an extreme brightness and contrast adjustment to facilitate the visualization of globules at the edge of the powder. (c) A magnified image of the small region identified by the rectangular box in (b).

Figure 3(a) is the native bright-field STEM image from the edge of a powder sample. In order to facilitate the visualization of globules, we applied an extreme brightness and contrast adjustment in Fig. 3(b), wherein the enlarged image of boxed region is shown in Fig. 3(c). The STEM images further evidence the existence of globules and their aggregates observed in the FE-SEM images.

Hydrogel structures of sample dialyzed in DIW and KOH

We investigated the impacts of different dialysis solutions for post-treatments on the structures of polyampholyte hydrogels. A piece of as-prepared PA-10-2.1 stored at room temperature was also quenched in liquid nitrogen and freeze-dried as shown in Figs. 4(a) and 4(b). Figures 4(c) and 4(d) show the

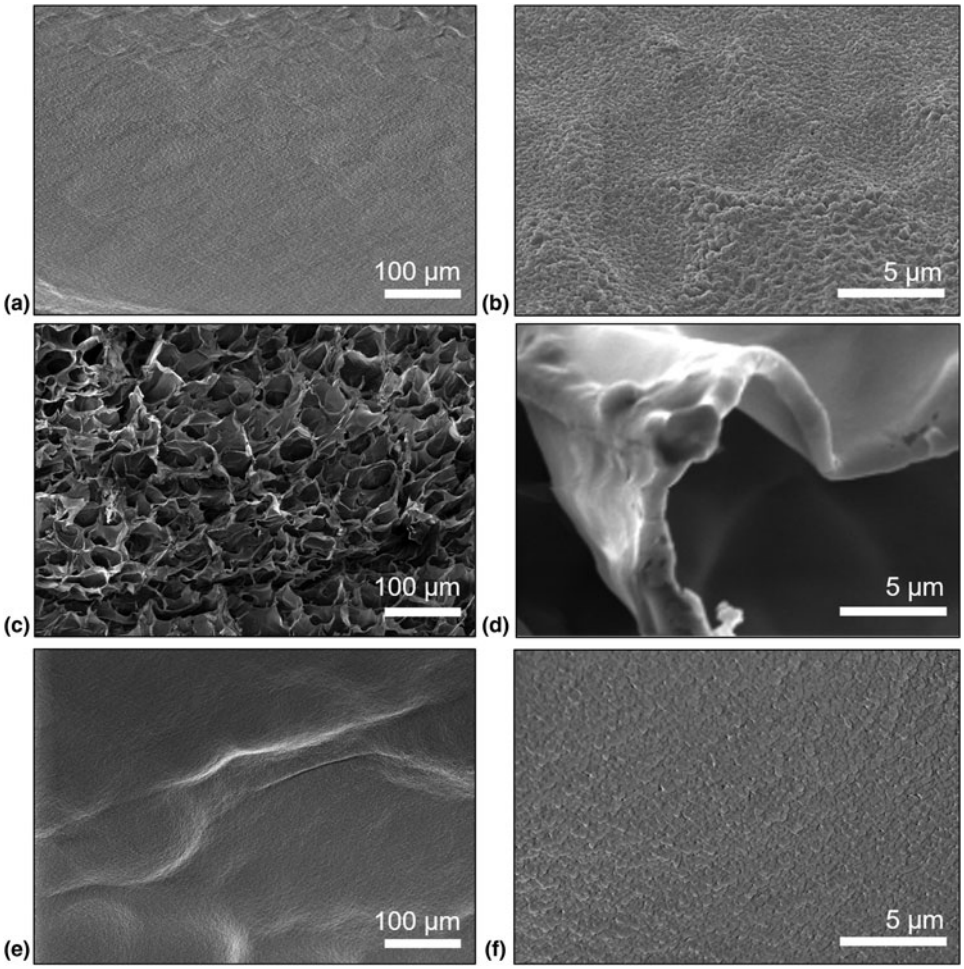

Figure 4. The SEM image of (a) freeze-dried PA-10-2.1, (c) freeze-dried D-PA-10-2.1, and (e) freeze-dried K-PA-10-2.1. The images (b), (d), and (f) are the zoomed-in images of (a), (c), and (e). All samples were quenched from +20 °C in liquid nitrogen, followed by freeze-drying processes.

https://doi.org/10.1557/mrc.2018.149

SEM images of DIW-dialyzed hydrogel of D-PA-10-2.1. The morphology of D-PA-10-2.1 turns into a microscopic cellular structure of polymeric networks with a pore size of ~20 μm after dialysis. The SEM result suggests that salt ions are essential to screen charges of the polymer chains and thereby prevent electrostatic attraction between the polymer chains. After removing NaCl, highly charged polymer chains with opposite charges collapse together.[29] In other words, the polyampholyte chains are "*zipped*" as water and the polymer separate from each other, resulting in the macroscopic structure in Fig. 4(c).[30]

The *zipping* of the polyampholyte chains is crucial to form a tough hydrogel. After the dialysis in DIW, the mobile ions (i.e., Na^+ and Cl^-) are leaching out from the hydrogel. This process facilitates the formation of ionic bonds between the oppositely charged groups in polyampholyte backbones.[21,22] Because of the interaction strength of ion bonds, strong and weak ionic bonds have distinguishable properties. Under tensile strain, the strong ionic associations serve as permanent crosslinking points, which keep the shape of the hydrogel. Meanwhile, weak ionic associations act as sacrificial bonds. They break during deformation and dissipate energy. After removing external force, the weak interactions are formed again.[22] This energy dissipation mechanism makes polyampholyte a class of tough hydrogel.[31]

According to the *zipping* mechanism described above, one can hypothesize that dialysis in a high ionic strength neutral salt solution may prevent the collapse of the chains. In our previous study, we used KOH as the solution for dialyzing as-prepared hydrogel because the KOH solutions are often used as a solution component for gel electrolytes in the electrochemical storage device.[16] The structures of quenched and freeze-dried K-PA-10-2.1 are shown in Figs. 4(e) and 4(f). The microscopic cellular structure shown in Fig. 4(c) is not observed when the polyampholyte is dialyzed in a 6 M KOH solution, indicating that the electrolyte exchange between NaCl with KOH prevented the *zipping*. For 6 M KOH case, the direct microscopic observation of globules in the freeze-dried hydrogel was not possible, probably due to the presence of large amount of KOH. Instead, we used indirect methods to obtain clues about nanoscopic morphology of K-PA-10-2.1 sample. In the supporting information, the SAXS fitting (Fig. S1) shows that the nanoscopic globular structures found in PA-10-2.1 sample[20] is also found in K-PA-10-2.1 sample. It is, however, notable that K-PA-10-2.1 samples showed whitening and stiffening after 6 M KOH dialysis, which may suggest the dissociation of amide group in MPTC monomeric unit in strong basic solution. Although further chemical analysis may provide molecular insight about the mechanism of whitening and stiffening, the SAXS result shows that there is no fundamental change in the nanoscopic structure of polymer chains.

The "*non-zipping*" of the polyampholyte chains in K-PA-10-2.1 is critical to enhance low-temperature ionic conductivity.[16,20] Because the globular structure in the polyampholyte hydrogel does not collapse into a microscopic cellular structure, the ice formation in the hydrogel is disrupted upon cooling. When ice forms, the water molecules in inter-globular regions firstly transform into ice. Water molecules trapped within the globules do not form ice because they cannot align themselves to form a periodic crystalline molecular alignment, due to either a strong confinement between the polymer chains or to a strong interaction with these chains. As ice crystals grow, the hydrated globules (i.e., polymer-rich domains), which do not participate in the ice formation, come closer to each other. Finally, ice crystals are inhibited from growing freely in size because of steric hindrance from the non-freezable globules and the polyampholyte networks between them that distribute across the entire hydrogel.[20] The *zipped* polymer chains in DIW-dialyzed D-PA-10-2.1 allow nearly monolithic growth of ice crystals in the hydrogel when cooled to freezing temperatures because of the large hollow space between microscopic cellular structures of the dialyzed polymer chains. The *non-zipped* polymer chains in PA-10-2.1 and K-PA-10-2.1, on the other hand, cause disrupted ice formation at the low temperatures, resulting in enhanced ionic conductivity as previously reported.[16,20]

Conclusion

In this study, we investigated the structure of a charge-balanced polyampholyte, poly(NaSS-*co*-NPTC) using low-dose FE-SEM and STEM, for the first time. Nanoscale globules in polyampholyte hydrogels were visualized; the globules has been theoretically predicted and experimentally supported by SAXS. In addition, we studied the impact of dialysis processes on microscopic structure of polymer networks, which is directly relevant to the mechanical properties and ice formation of the polyampholyte hydrogels. The structure of hydrogels dialyzed in DIW suggests the *zipping* trend of the polyampholyte chains, which is crucial to form a tough hydrogel. After removing NaCl, highly charged polymer chains with opposite charges collapse (or *zip*) to form microscopic (pore sizes of 10s of μm) cellular structure. The zipped polymer chain structure is crucial to make a tough hydrogel.[22] Such zipping phenomenon is not found when the as-prepared hydrogel was dialyzed in 6 M KOH solution. There is no visible microscopic structure in the KOH-dialyzed sample; the absence of microscopic structure is helpful in achieving disrupted ice formation at low temperatures.[16,20]

Supplementary material

The supplementary material for this article can be found at https://doi.org/10.1557/mrc.2018.149

Acknowledgments

The authors gratefully acknowledge funding from a NSERC DG (RGPIN 435914). Material characterization was partly done in the shared facility of the NanoFAB in the Faculty of Engineering at the University of Alberta. The use of the Advanced Photon Source was supported by the US DOE under Contract DE-AC02-06CH11357.

References

1. H. Jinnai, T. Higuchi, X. Zhuge, A. Kumamoto, K.J. Batenburg, and Y. Ikuhara: Three-dimensional visualization and characterization of polymeric self-assemblies by transmission electron microtomography. *Acc. Chem. Res.* **50**, 1293 (2017).
2. H-J. Chung, K. Ohno, T. Fukuda, and R.J. Composto: Self-regulated structures in nanocomposites by directed nanoparticle assembly. *Nano Lett.* **5**, 1878 (2005).
3. K.M. Beers and N.P. Balsara: Design of cluster-free polymer electrolyte membranes and implications on proton conductivity. *ACS Macro Lett.* **1**, 1155 (2012).
4. D.V. Krogstad, S-H. Choi, N.A. Lynd, D.J. Audus, S.L. Perry, J.D. Gopez, C.J. Hawker, E.J. Kramer, and M.V. Tirrell: Small angle neutron scattering study of complex coacervate micelles and hydrogels formed from ionic diblock and triblock copolymers. *J. Phys. Chem. B* **118**, 13011 (2014).
5. D. Lolla, J. Gorse, C. Kisielowski, J. Miao, P.L. Taylor, G.G. Chase, and D. H. Reneker: Polyvinylidene fluoride molecules in nanofibers, imaged at atomic scale by aberration corrected electron microscopy. *Nanoscale* **8**, 120 (2016).
6. M. Shibayama: Structure-mechanical property relationship of tough hydrogels. *Soft Matter* **8**, 8030 (2012).
7. B. Sierra-Martin, J.R. Retama, M. Laurenti, A. Fernández Barbero, and E. López Cabarcos: Structure and polymer dynamics within pnipam-based microgel particles. *Adv. Colloid Interface Sci.* **205**, 113 (2014).
8. B. Trappmann, J.E. Gautrot, J.T. Connelly, D.G.T. Strange, Y. Li, M. L. Oyen, M.A. Cohen Stuart, H. Boehm, B. Li, V. Vogel, J.P. Spatz, F. M. Watt, and W.T.S. Huck: Extracellular-matrix tethering regulates stem-cell fate. *Nat. Mater.* **11**, 642 (2012).
9. H. Yuan, J. Xu, E.P. van Dam, G. Giubertoni, Y.L.A. Rezus, R. Hammink, H.J. Bakker, Y. Zhan, A.E. Rowan, C. Xing, and P.H.J. Kouwer: Strategies to increase the thermal stability of truly biomimetic hydrogels: combining hydrophobicity and directed hydrogen bonding. *Macromolecules* **50**, 9058 (2017).
10. O. Zavgorodnya, C.A. Carmona-Moran, V. Kozlovskaya, F. Liu, T.M. Wick, and E. Kharlampieva: Temperature-responsive nanogel multilayers of poly (n-vinylcaprolactam) for topical drug delivery. *J. Colloid Interface Sci.* **506**, 589 (2017).
11. C. Hamngren Blomqvist, T. Gebäck, A. Altskär, A.M. Hermansson, S. Gustafsson, N. Lorén, and E. Olsson: Interconnectivity imaged in three dimensions: nano-particulate silica-hydrogel structure revealed using electron tomography. *Micron* **100**, 91 (2017).
12. A.V. Dobrynin, R.H. Colby, and M. Rubinstein: Polyampholytes. *J. Polym. Sci. Part B Polym. Phys.* **42**, 3513 (2004).
13. S.E. Kudaibergenov: Recent advances in the study of synthetic polyampholytes in solutions. *Adv. Polym. Sci.* **114**, 115 (1999).
14. A.B. Ihsan, T.L. Sun, T. Kurokawa, S.N. Karobi, T. Nakajima, T. Nonoyama, C.K. Roy, F. Luo, and J.P. Gong: Self-healing behaviors of tough polyampholyte hydrogels. *Macromolecules* **49**, 4245 (2016).
15. J. Niskanen and H. Tenhu: How to manipulate the upper critical solution temperature (Ucst)? *Polym. Chem.* **8**, 220 (2017).
16. X. Li, L. Liu, X. Wang, Y.S. Ok, J.A.W. Elliott, S.X. Chang, and H-J. Chung: Flexible and self-healing aqueous supercapacitors for low temperature applications: polyampholyte gel electrolytes with biochar electrodes. *Sci. Rep.* **7**, 1685 (2017).
17. T-G. La, X. Li, A. Kumar, Y. Fu, S. Yang, and H-J. Chung: Highly flexible, multipixelated thermosensitive smart windows made of tough hydrogels. *ACS Appl. Mater. Interfaces* **9**, 33100 (2017).
18. P.G. Higgs and J.F. Joanny: Theory of polyampholyte solutions. *Chem. Phys.* **94**, 1543 (1991).
19. G. Nisato, J. Munch, and S. Candau: Swelling, structure, and elasticity of polyampholyte hydrogels. *Langmuir* **15**, 4236 (1999).
20. X. Li, H. Charaya, G.M. Bernard, J.A.W. Elliott, V.K. Michaelis, B. Lee, and H-J. Chung: Low-temperature ionic conductivity enhanced by disrupted ice formation in polyampholyte hydrogels. *Macromolecules* **51**, 2723 (2018).
21. A.B. Ihsan, T.L. Sun, S. Kuroda, M.A. Haque, T. Kurokawa, T. Nakajima, and J.P. Gong: A phase diagram of neutral polyampholyte – from solution to tough hydrogel. *J. Mater. Chem. B* **1**, 4555 (2013).
22. T.L. Sun, T. Kurokawa, S. Kuroda, A.B. Ihsan, T. Akasaki, K. Sato, H. A. Haque, T. Nakajima, and J.P. Gong: Physical hydrogels composed of polyampholytes demonstrate high toughness and viscoelasticity. *Nat. Mater.* **12**, 932 (2013).
23. T. Egerton, P. Li, and M. Malac: Radiation damage in the tem and sem. *Micron* **35**, 399 (2004).
24. D. Grubb: Radiation damage and electron microscopy of organic polymers. *J. Mater. Sci.* **9**, 1715 (1974).
25. G. Michler and R. Godehardt: *Electron Microscopy of Polymers* (Springer-Verlag, Berlin, Heidelberg, 2008).
26. J.N. Hunt, K.E. Feldman, N.A. Lynd, J. Deek, L.M. Campos, J.M. Spruell, B.M. Hernandez, E.J. Kramer, and C.J. Hawker: Tunable, high modulus hydrogels driven by ionic coacervation. *Adv. Mater.* **23**, 2327 (2011).
27. W. MacKnight, W. Taggart, and R. Stein: A model for the structure of ionomers. *J. Polym. Sci. Polym. Symp.* **45**, 113 (1974).
28. T. Gierke, G. Munn, and F. Wilson: The morphology in nafion perfluorinated membrane products, as determined by wide- and small-angle x-ray studies. *J. Polym. Sci. Polym. Phys. Ed.* **19**, 1687 (1981).
29. R. Kumar and G.H. Fredrickson: Theory of polyzwitterion conformations. *J. Chem. Phys.* **131**, 104901 (2009).
30. J. Deek, P.J. Chung, J. Kayser, A.R. Bausch, and C.R. Safinya: Neurofilament sidearms modulate parallel and crossed-filament orientations inducing nematic to isotropic and re-entrant birefringent hydrogels. *Nat. Commun.* **4**, 2224 (2013).
31. J-Y. Sun, X. Zhao, W.R. Illeperuma, O. Chaudhuri, K.H. Oh, D.J. Mooney, J.J. Vlassak, and Z. Suo: Highly stretchable and tough hydrogels. *Nature* **489**, 133 (2012).

https://doi.org/10.1557/mrc.2018.149

Supplementary Material

Direct Visualization of Nano and Microscale Polymer Morphologies in As-Prepared and Dialyzed Polyampholyte Hydrogels by Electron Microscopy Techniques

Xinda Li[1], Hemant Charaya[1], Thuy Nguyen Thanh Tran[1], Byeongdu Lee[2], Jae-Young Cho[3], Hyun-Joong Chung[1,*]

[1]Department of Chemical and Materials Engineering, University of Alberta, Edmonton, Alberta T6G 1H9, Canada

[2]Advanced Photon Source, Argonne National Laboratory, Argonne, Illinois 60439, United States

[3]National Research Council of Canada (NRC), 11421 Saskatchewan Drive NW, Edmonton, Alberta T6G 2M9, Canada

* Address all correspondence to Hyun-Joong Chung at chung.hj13@ualbrerta.ca

Polyampholyte Hydrogel Synthesis. The protocol of polyampholyte synthesis was described in previous works.[S1] Briefly, 1 M Sodium 4-vinylbenzenesulfonate (NaSS) and 1 M [3-(methacryloylamino)propyl] trimethylammonium chloride (MPTC) with Irgacure 2959 (photoinitiator, 0.25 mol%, compared to the total concentration of NaSS and MPTC) and NaCl were dissolved in deionized water to form the precursor solution. In the precursor solution, NaCl concentration is 10 wt%. Here, sodium and chloride ions in the monomers of NaSS and MPTC were accounted into the total concentration. The aqueous precursor solution was injected into the gap between two glass plates separated by a 1 mm thick spacer, followed by polymerization initiated by irradiating the sample with UV light with a lamp-to-sample distance of 5 mm (broadband light with a maximum peak at 365 nm with the intensity of 22 mW/cm^2, Jelight UVO-Cleaner Model-342, US). The list of prepared samples are in Table 1. Here, we denote the samples using the code PA-#-*c*, where the # is the NaCl concentration (wt%) in the polyampholyte hydrogel, *c* is the total monomer concentration (M). The NaCl concentration in the as-prepared hydrogel is calculated as:

$$C_{\mathrm{NaCl}} = \frac{m_{\mathrm{NaCl}}}{m_{\mathrm{NaCl}}+m_{\mathrm{water}}} \times 100\% \qquad (1)$$

where m_{NaCl} is the total mass of NaCl, and m_{water} is the mass of water added in the precursor solution. It is noted that NaSS and MPTC contain sodium and chloride ions, respectively which were accounted in the calculation for the m_{NaCl} value.

Small Angle X-Ray Scattering (SAXS) Characterization. SAXS samples were made by irradiating bees wax sealed glass capillaries (Charles Supper, US) containing a precursor solution with UV. After polymerization, one end of the glass capillary was manually broken and dialyzed in the 6 M KOH solution for one week to prepare K-PA-10-2.1. The SAXS experiments were performed with the beamline 12-ID-B of the Advanced Photon Source at the Argonne National Laboratory in the US. The 14 keV X-ray beam was exposed to the 1.5 mm diameter capillary

sample with an exposure time of typically 0.1 s. Scattered X-ray photons were measured with a Pilatus 2M (Dectris Ltd.) detector located about 2 m downstream of the sample. Ten images per sample were collected and averaged to confirm that no beam damage had occurred and to increase counting statistics. Background scattering from a capillary containing water was subtracted from sample data. The SAXS data in Figure S1 was fitted using our fitting model developed in our earlier study; details are in the reference [S1]. The fitting result was shown in Table S1, where f_p is the number concentration (*e.g.*, molar concentration) of primary particles. D_f is the fractal power-law. $\bar{R}_p$ and σ_p are the mean radius and variance of the external size of the primary particles, respectively. $R_{g,p}$ is the radius of gyration of the primary particle calculated from $\bar{R}_p$ and σ_p. $R_{g,c}$ and P are radius of gyration and the Porod constant of the cluster, respectively. v is the volume fraction of the primary particles in a cluster, respectively. The $R_{g,p}$ value of PA-10-2.1 is different from Reference [S1], where we calculated the value assuming solid spheres to emphasize the external size, whereas in the current analysis we used the original formula in Reference [S2] taking into account porous nature of the sphere.

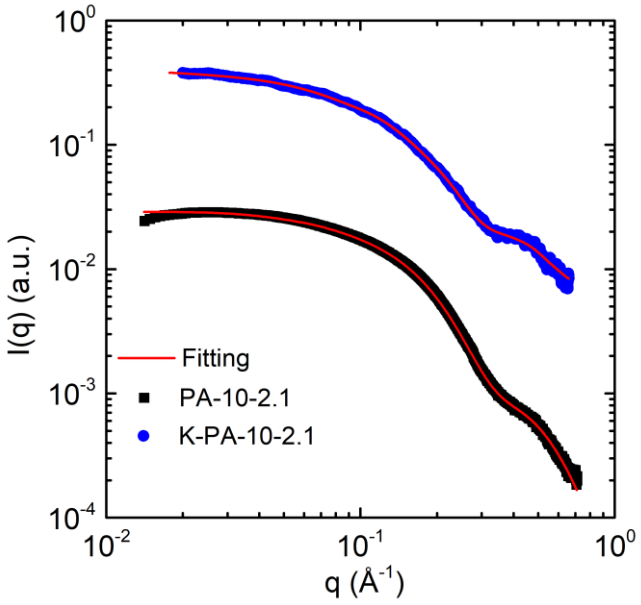

Figure S1 SAXS data for PA-10-2.1, K-PA-10-2.1. Here, the subtracted background are the capillaries filled with 10 wt% NaCl and 6 M KOH solution for PA-10-2.1 and K-PA-10-2.1, respectively. The red lines are the fits of the experimental data.

Table S1 Fitting parameters for SAXS results.

Sample	Cluster				Primary Particle (globule)				
	f	$R_{g,c}$(Å)	P	v(%)	f_p(a.u.)	$\bar{R}_p$(Å)	σ_p(Å)	D_f	$R_{g,p}$(Å)
K-PA-10-2.1	1.6	13.1	3.2	0	0.232	19.9	3.7	1.5	9.91
PA-10-2.1	1.2	13.1	1.2	0	0.024	18.1	4.7	1.8	9.56

References for Supporting Information

S1. X. Li, H. Charaya, G.M. Bernard, J.A.W. Elliott, V.K. Michaelis, B. Lee, H-J. Chung: Low-Temperature Ionic Conductivity Enhanced by Disrupted Ice Formation in Polyampholyte Hydrogels. *Macromolecules* **51**, 2723-2731 (2018).

S2. R. Besselink and J.E. ten Elshof: Mass-fractal growth in niobia/silsesquioxane mixtures: a small-angle X-ray scattering study. *Journal of Applied Crystallography* **47**, 1606-1613 (2014).